Supplementary Information

Selective conversion of alcohols in water to carboxylic acids by *in situ* generated ruthenium *trans* dihydrido carbonyl PNP complexes

Jong-Hoo Choi,[a] Leo E. Heim,[a] Mike Ahrens,[b] and Martin H. G. Prechtl[a,]*

[a] Department of Chemistry, University of Cologne, Greinstr.6,50939 Cologne, Germany.
Fax: +49 221 470 1788; Tel: +49 221 470 1981;
E-mail: martin.prechtl@uni-koeln.de Web: www.catalysislab.de
[b] Institute of Chemistry, Humboldt University at Berlin, Brook-Taylor-Straße 2, D-12489 Berlin, Germany.

Table of contents

1. Online gas-phase mass spectrometry of the alcohol decarbonylation by complex 3 4

   Fig. S1 MS-monitoring of the decarbonylation reaction of ethanol (black) and ethanol-d6 (red) by 0.2 mmol complex 2. Diagram shows the detected averaged distribution of evolved hydrocarbons. 4

   Fig. S2 MS-monitoring of the decarbonylation reaction of pentanol by 0.2 mmol complex 2. Diagram shows the detected averaged distribution of evolved hydrocarbons. 4

2. LIFDI-MS analysis of complexes 3, 4a, 4b and 6 5

   Fig. S3 LIFDI-MS (Argon collided) of [RuH_2(CO)(Me-PNP)] 3 (black, 501 – 511)in toluene compared to simulated isotope pattern of [RuH_2(CO)(Me-PNP)] 507 (red, 501 – 511). Retention time (RT) 2.14 min of 7.00 min. 5

   Fig. S4 Simulated istope pattern of fragment [RuH(CO)(Me-PNP)] 500 – 509 5

   Fig. S5 Simulated istope pattern of fragment [Ru(CO)(Me-PNP)] 499 – 508. 6

   Fig. S6 LIFDI-MS/MS of [RuH(CO)(Me-PNP)] 506 (black, 501 – 509) in toluene decomposed from complex 4a under MS conditions compared to simulated isotope pattern of [RuH(CO)(Me-PNP)] 506 (red, 501 – 509). RT 5.23 min of 7.00 min. Compared to the simulated isotope pattern of [RuH(CO(Me-PNP)] 506 m/z in red, the detected fragment differs slightly towards lower mass value, which can be explained by the detection of a fragmentation mixture of the species [Ru(CO)(Me-PNP)] 505 (see simulated isotope pattern in Fig. S5) and [RuH(CO)(Me-PNP)] 506. 6

   Fig. S7 Simulated istope pattern of fragment [Ru(CO)($OOCCH_3$)(Me-PNP)] 558 – 569. 7

   Fig. S8 LIFDI-MS/MS of [RuH(CO)(PNP)] 6 (black, 485 – 495)in toluene compared to simulated isotope pattern of [RuH(CO)(PNP)] 491 (red, 485 – 495). Retention time (RT) 2.61 min of 7.00 min. 7

   Fig. S9 Simulated istope pattern of fragment [Ru(CO)(PNP)] 484 – 494 8

3. IR spectra of complexes 3, 4a, 4b and 7 9

   Fig. S10 IR spectra of [RuH_2(CO)(Me-PNP)] 3 (black) and [$RuH_2(^{13}CO)$(Me-PNP)] 3 (red). 9

   Fig. S11 IR spectrum of [RuH(CO)(hexanolate)(Me-PNP)] 4a. 9

   Fig. S12 IR spectrum of [RuH(CO)($OOCCH_3$)(Me-PNP)] 4b. 10

   Fig. S13 IR spectra of [RuH(CO)(PNP)] 6 (black) and [RuH(^{13}CO)(PNP)] 6 (red). 10

4. NMR spectra of complexes 3, 4a, 4b and 6 11

   Fig. S14 ^1H-NMR of [RuH_2(CO)(Me-PNP)] 3 in C_6D_6 at 600 MHz 11

   Fig. S15 $^{13}C_{APT}$-NMR of 3 in C_6D_6 at 75 MHz. 11

   Fig. S16 $^{13}C_{APT}$-NMR of [$RuH_2(^{13}CO)$(Me-PNP)] 3 at 75 MHz. 12

   Fig. S17 ^1H-NMR of [RuH(CO)(hexanolate)(Me-PNP)] 4a in C_6D_6 at 600 MHz 12

   Fig. S18 ^{13}C-deptQ-NMR of [RuH(CO)(hexanolate)(Me-PNP)] 4a in C_6D_6 at 150 MHz. 13

   Fig. S19 H,C HMQC of [RuH(CO)(hexanolate)(Me-PNP)] 4a in C_6D_6 at 600 MHz (^1H) 150 MHz (^{13}C). 13

Fig. S20 ^{1}H-NMR of [RuH(CO)(OOCCH$_3$)(Me-PNP)] 4b in C_6D_6 at 600 MHz. 14

Fig. S21 ^{13}C-deptQ-NMR of [RuH(CO)(OOCCH$_3$)(Me-PNP)] 4b in C_6D_6 at 150 MHz. 14

Fig. S22 H,C HMQC of [RuH(CO)(OOCCH$_3$)(Me-PNP)] 4b in C_6D_6 at 600 MHz (^{1}H)/150 MHz (^{13}C). 15

Fig. S23 ^{1}H-NMR of [RuH(CO) (PNP)] 6 in C_6D_6 at 300 MHz. 15

Fig. S24 $^{13}C_{APT}$-NMR of [RuH(CO) (PNP)] 6 in C_6D_6 at 75 MHz. 16

Fig. S 25 $^{13}C_{APT}$-NMR of [RuH(^{13}CO) (PNP)] 6 in C_7D_8 at 75 MHz. 16

Fig. S26 ^{31}P{^{1}H}-NMR of [RuH(CO) (PNP)] 6 in C_6D_6 at 121 MHz. 17

Fig. S27 ^{1}H-NMR of complex 7 in C_6D_6 at 300 MHz. Hydrogenation of complex 6 to complex 7 with 1.5 bar H_2. 17

Fig. S28 ^{31}P{^{1}H}-NMR of complex 7 in C_6D_6 at 121 MHz. Hydrogenation of complex 6 to complex 7 with 1.5 bar H_2, 79% conversion. 18

5. Single Chrystal structure of complex 4b 19

Fig. S29 ORTEP diagram of the single crystal structure of complex 4b. Ellipsoids are illustrated at 50% possibility. All hydrogen atoms not depicted here except for H1 for clarity. 19

1. Online gas-phase mass spectrometry of the alcohol decarbonylation by complex 3

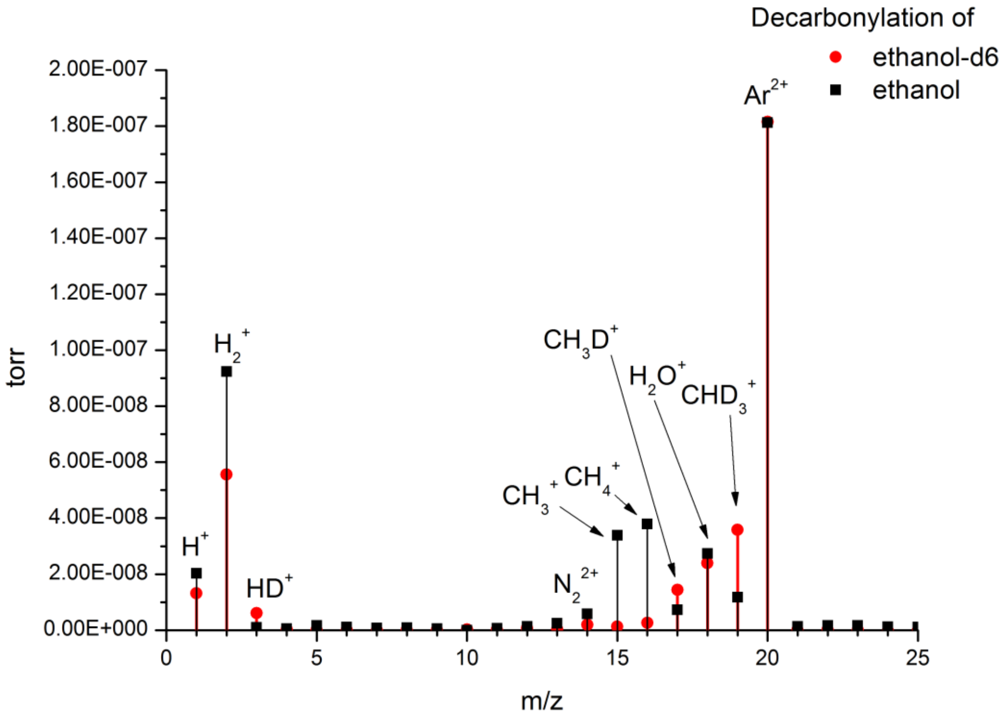

Fig. S1 MS-monitoring of the decarbonylation reaction of ethanol (black) and ethanol-d6 (red) by 0.2 mmol complex **2**. Diagram shows the detected averaged distribution of evolved hydrocarbons.

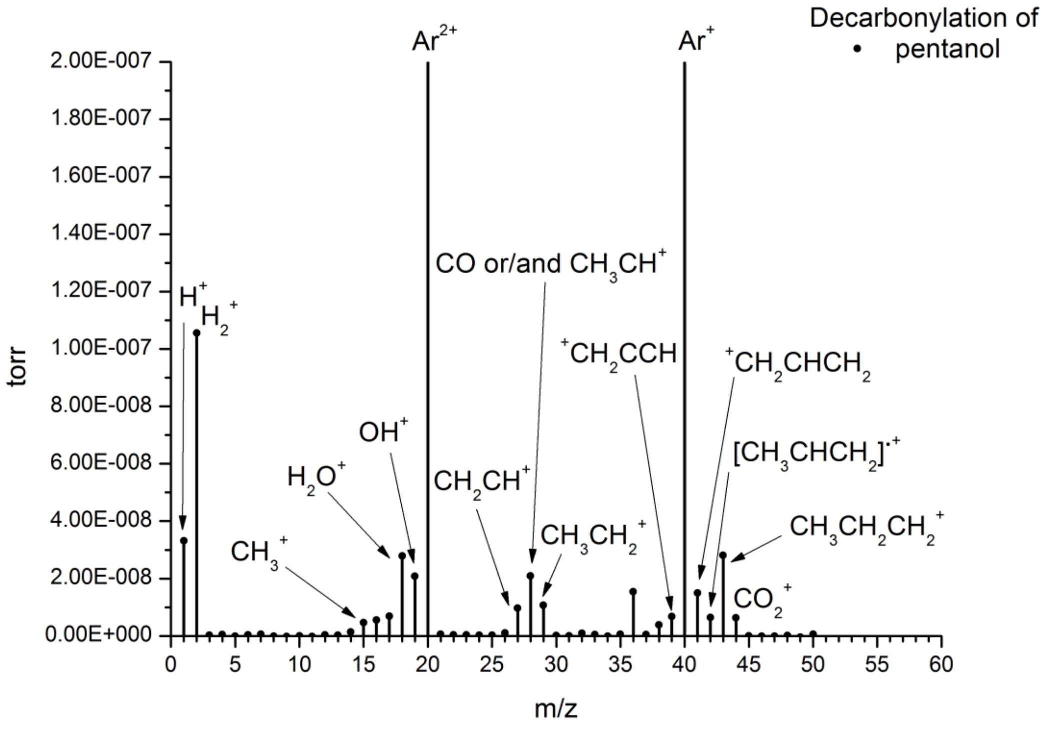

Fig. S2 MS-monitoring of the decarbonylation reaction of pentanol by 0.2 mmol complex **2**. Diagram shows the detected averaged distribution of evolved hydrocarbons.

2. LIFDI-MS analysis of complexes 3, 4a, 4b and 6

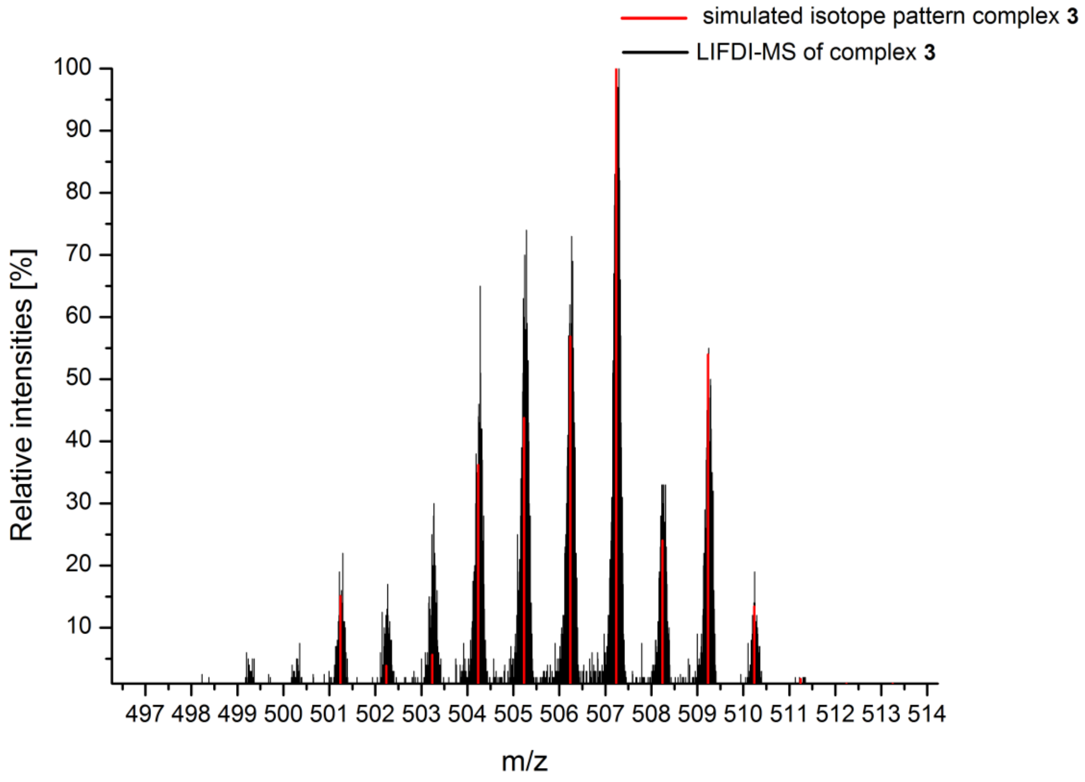

Fig. S3 LIFDI-MS (Argon collided) of [RuH$_2$(CO)(Me-PNP)] **3** (black, 501 – 511)in toluene compared to simulated isotope pattern of [RuH$_2$(CO)(Me-PNP)] 507 (red, 501 – 511). Retention time (RT) 2.14 min of 7.00 min.

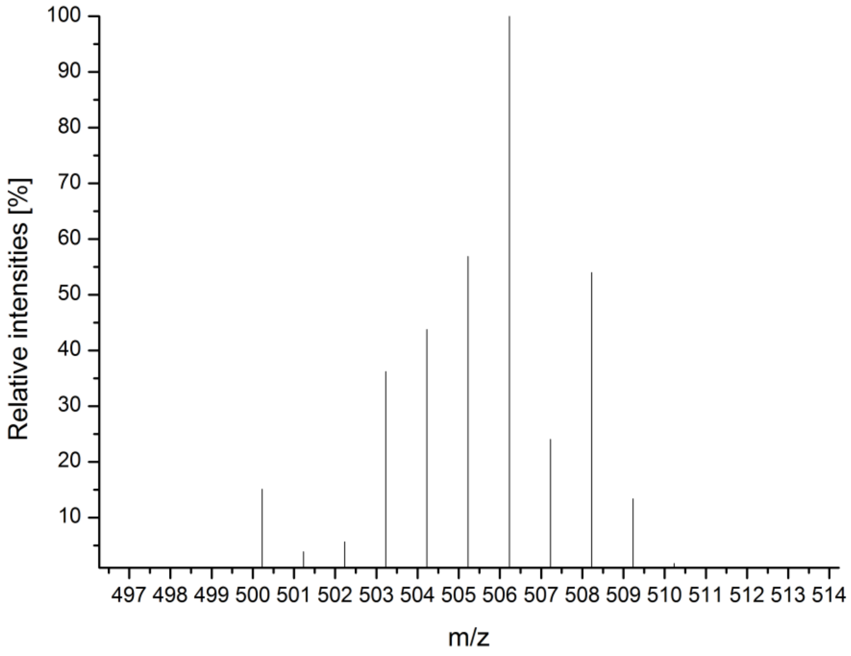

Fig. S4 Simulated istope pattern of fragment [RuH(CO)(Me-PNP)] 500 – 509.

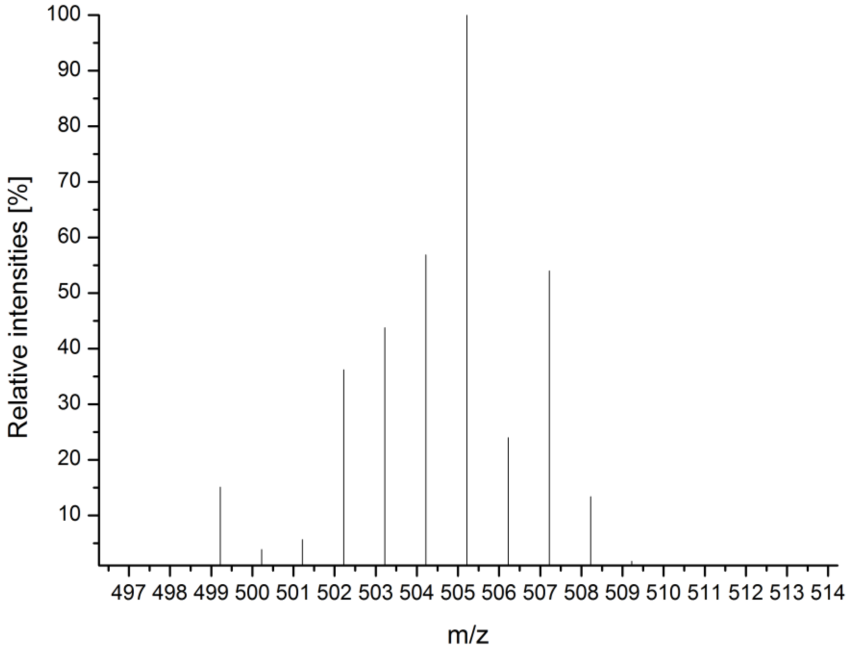

Fig. S5 Simulated istope pattern of fragment [Ru(CO)(Me-PNP)] 499 – 508.

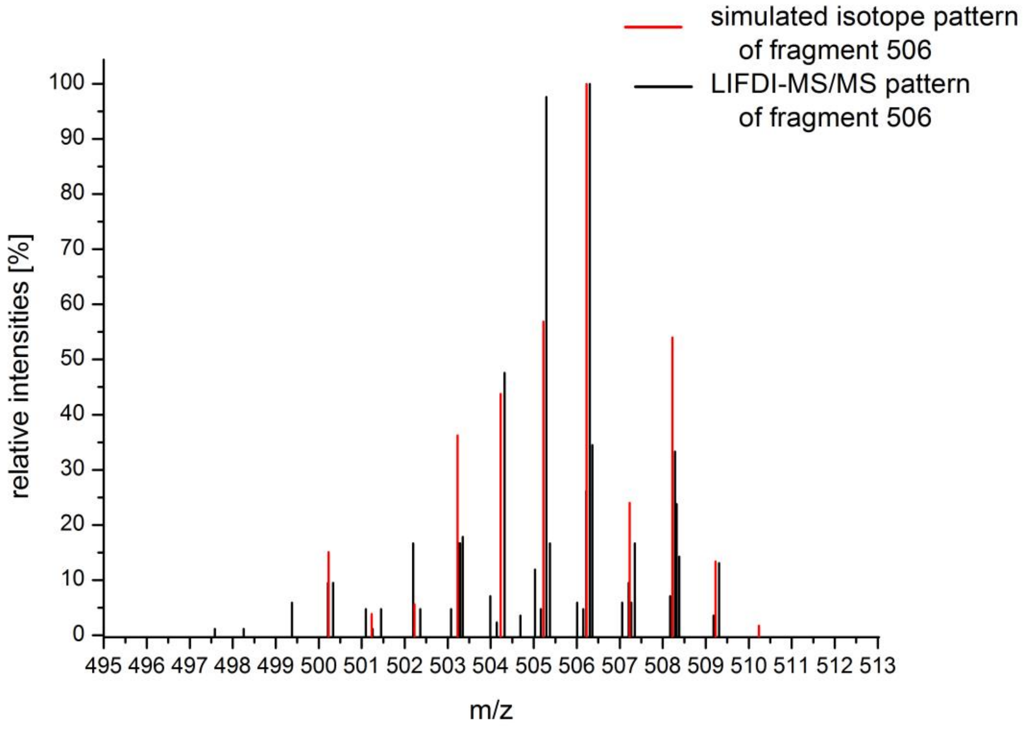

Fig. S6 LIFDI-MS/MS of [RuH(CO)(Me-PNP)] 506 (black, 501 – 509) in toluene decomposed from complex **4a** under MS conditions compared to simulated isotope pattern of [RuH(CO)(Me-PNP)] 506 (red, 501 – 509). RT 5.23 min of 7.00 min. Compared to the simulated isotope pattern of [RuH(CO(Me-PNP)] 506 m/z in red, the detected fragment differs slightly towards lower mass value, which can be explained by the detection of a fragmentation mixture of the species [Ru(CO)(Me-PNP)] 505 (see simulated isotope pattern in Fig. S5) and [RuH(CO)(Me-PNP)] 506.

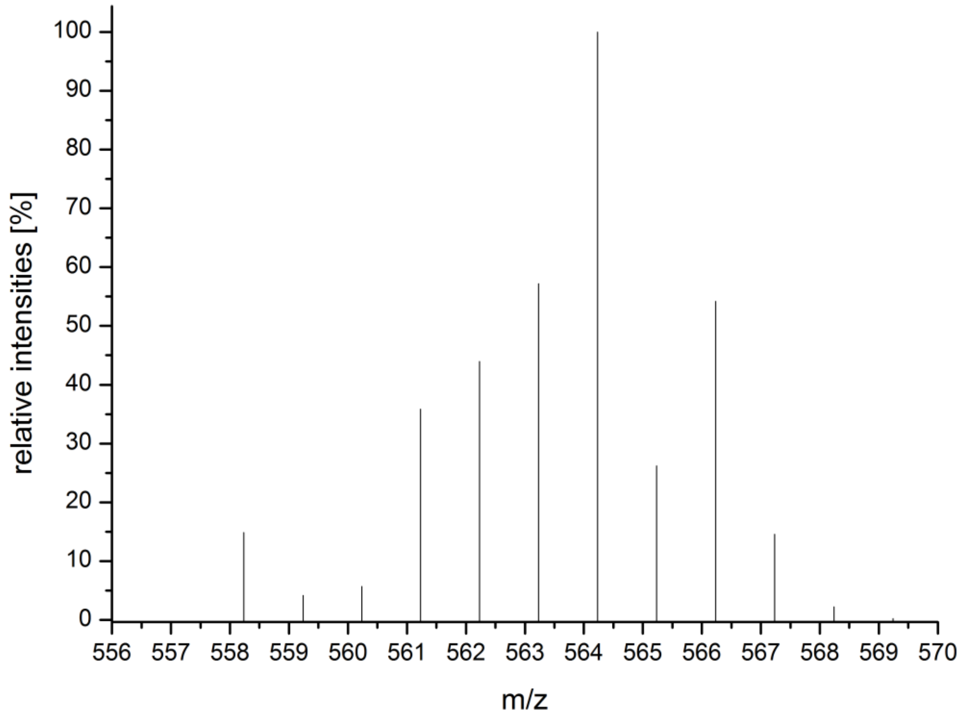

Fig. S7 Simulated istope pattern of fragment [Ru(CO)(OOCCH$_3$)(Me-PNP)] 558 – 569.

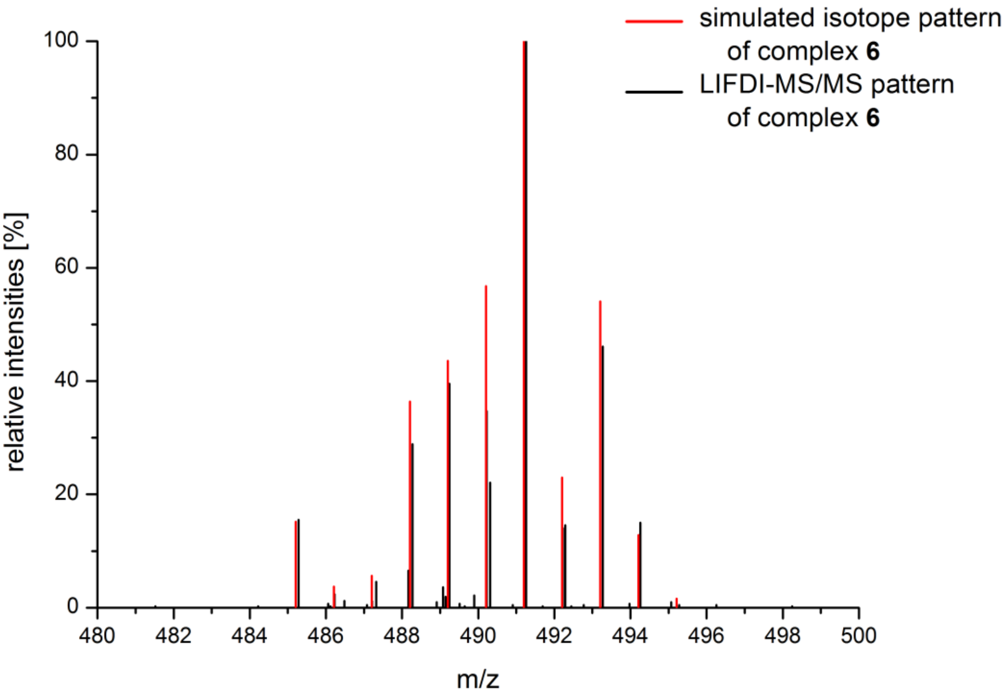

Fig. S8 LIFDI-MS/MS of [RuH(CO)(PNP)] **6** (black, 485 – 495)in toluene compared to simulated isotope pattern of [RuH(CO)(PNP)] 491 (red, 485 – 495). Retention time (RT) 2.61 min of 7.00 min.

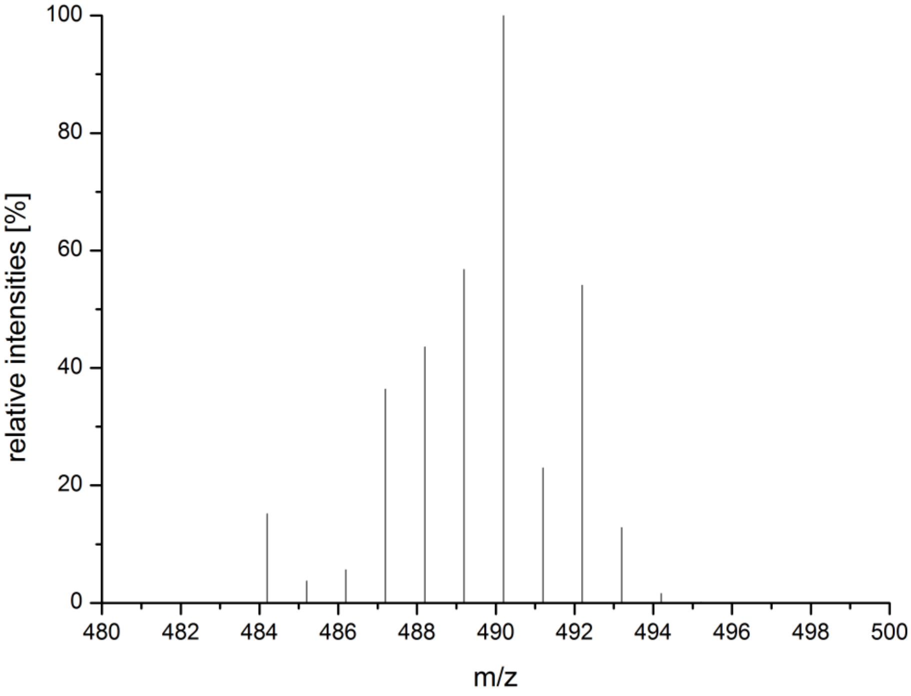

Fig. S9 Simulated istope pattern of fragment [Ru(CO)(PNP)] 484 – 494.

3. IR spectra of complexes 3, 4a, 4b and 7

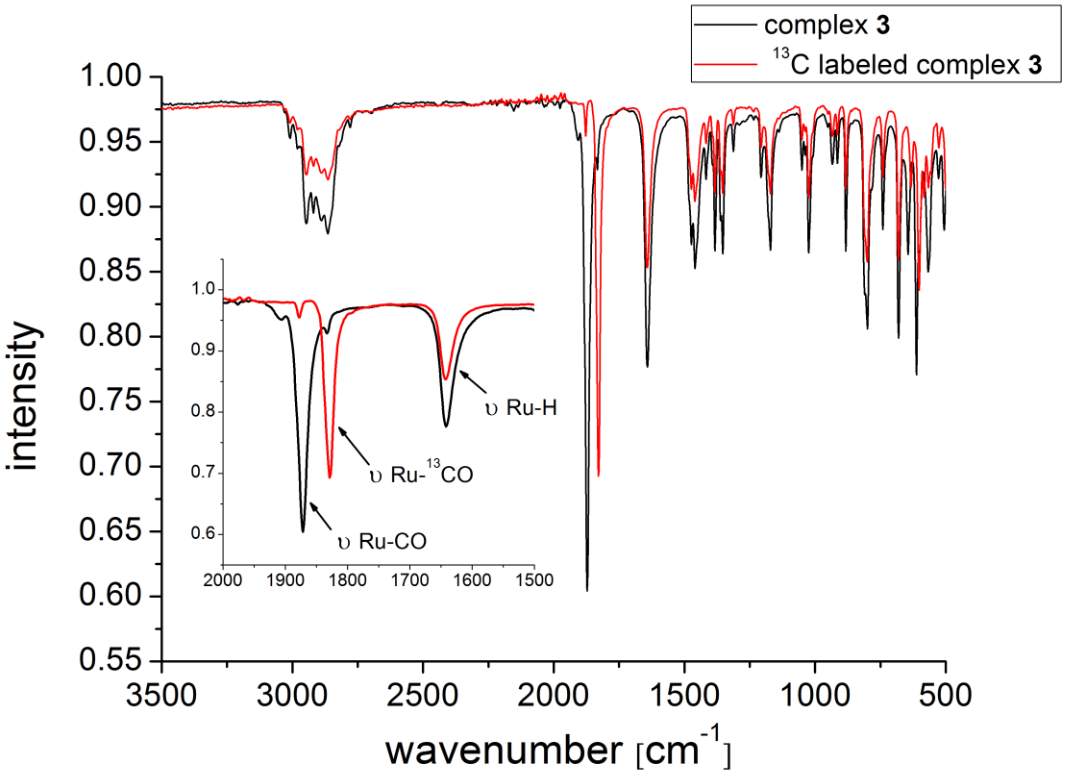

Fig. S10 IR spectra of [RuH$_2$(CO)(Me-PNP)] **3** (black) and [RuH$_2$(^{13}CO)(Me-PNP)] **3** (red).

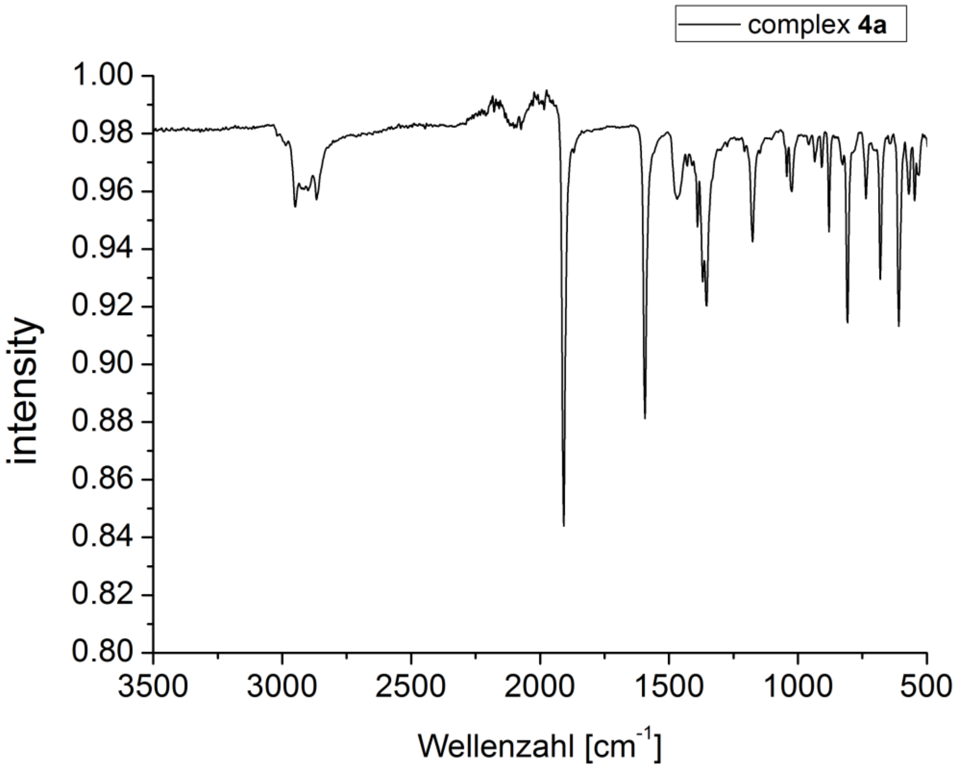

Fig. S11 IR spectrum of [RuH(CO)(hexanolate)(Me-PNP)] **4a**.

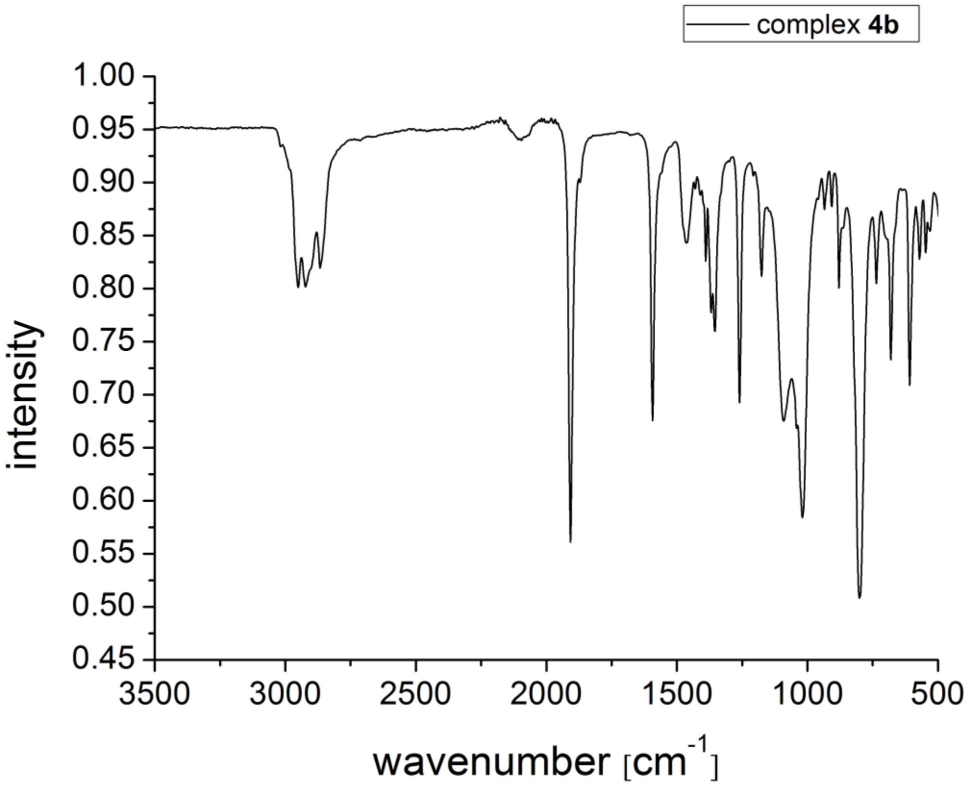

Fig. S12 IR spectrum of [RuH(CO)(OOCCH$_3$)(Me-PNP)] **4b**.

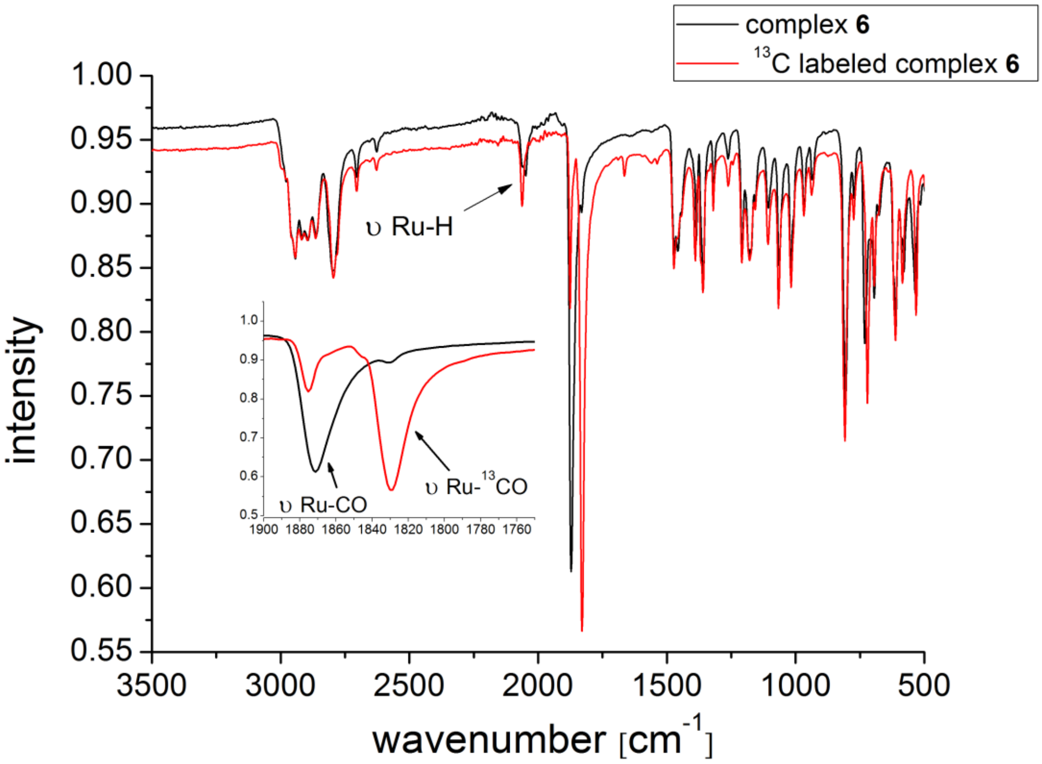

Fig. S13 IR spectra of [RuH(CO)(PNP)] **6** (black) and [RuH(^{13}CO)(PNP)] **6** (red).

4. NMR spectra of complexes 3, 4a, 4b and 6

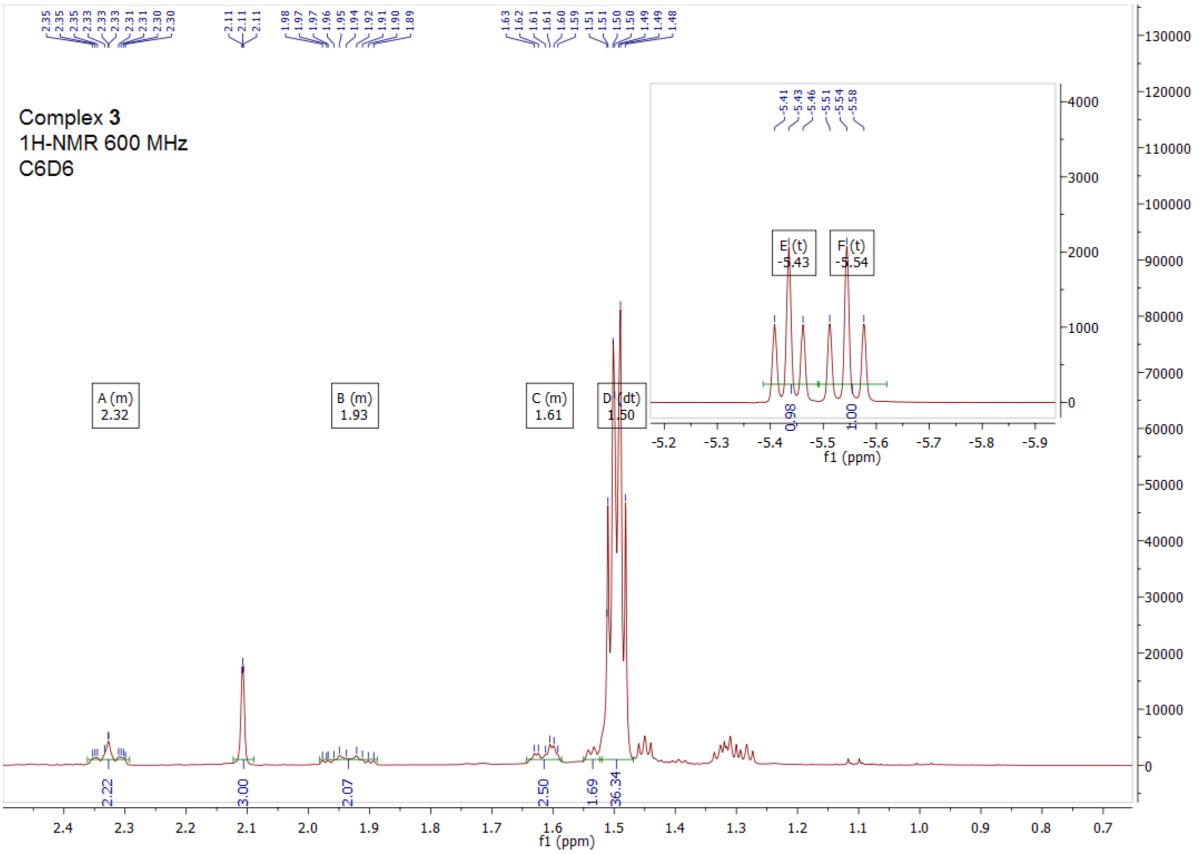

Fig. S14 ^{1}H-NMR of [RuH$_2$(CO)(Me-PNP)] **3** in C_6D_6 at 600 MHz.

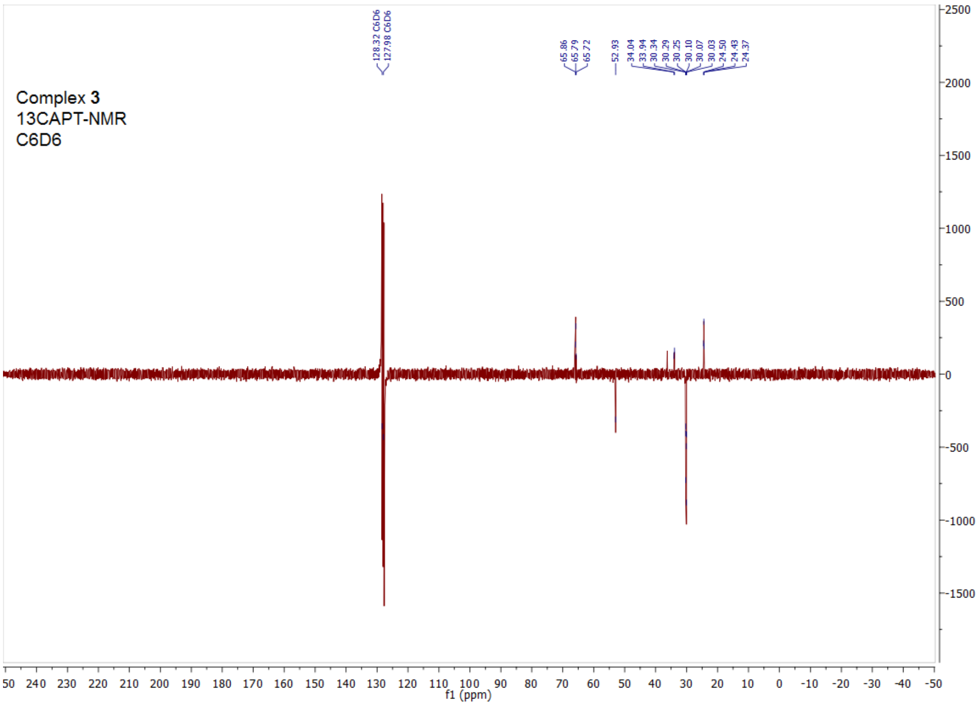

Fig. S15 $^{13}C_{APT}$-NMR of **3** in C_6D_6 at 75 MHz.

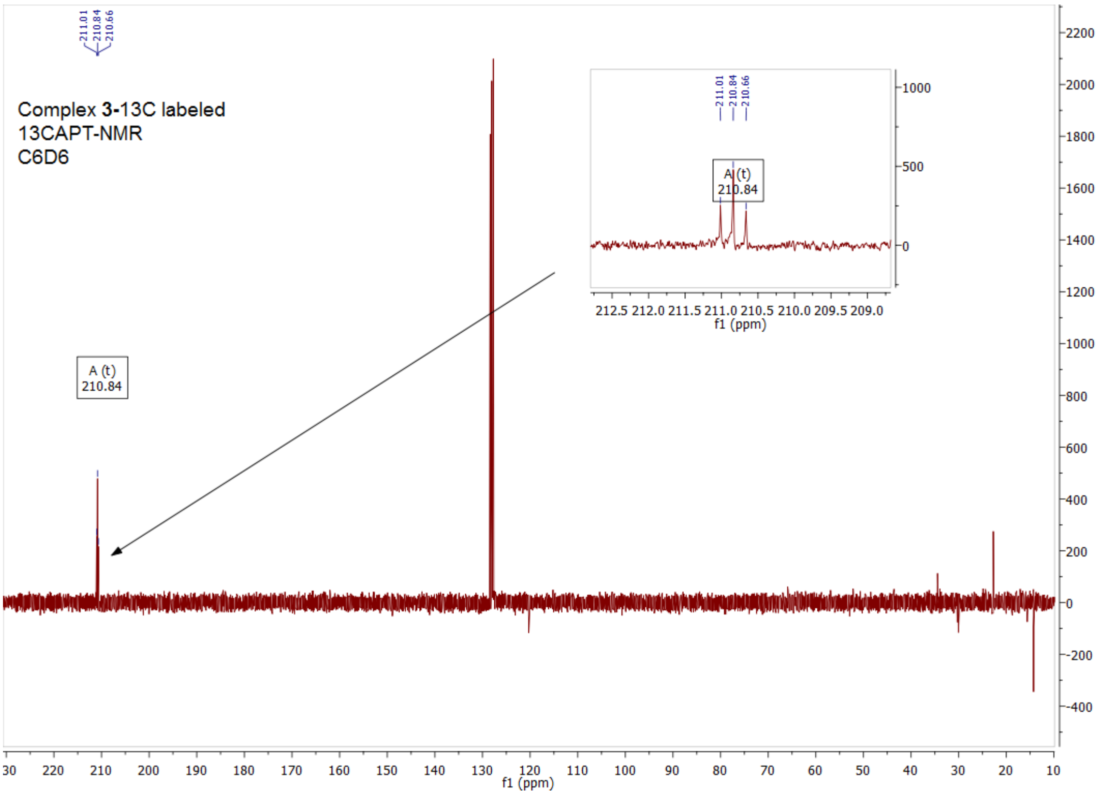

Fig. S16 $^{13}C_{APT}$-NMR of $[RuH_2(^{13}CO)(Me\text{-}PNP)]$ **3** at 75 MHz.

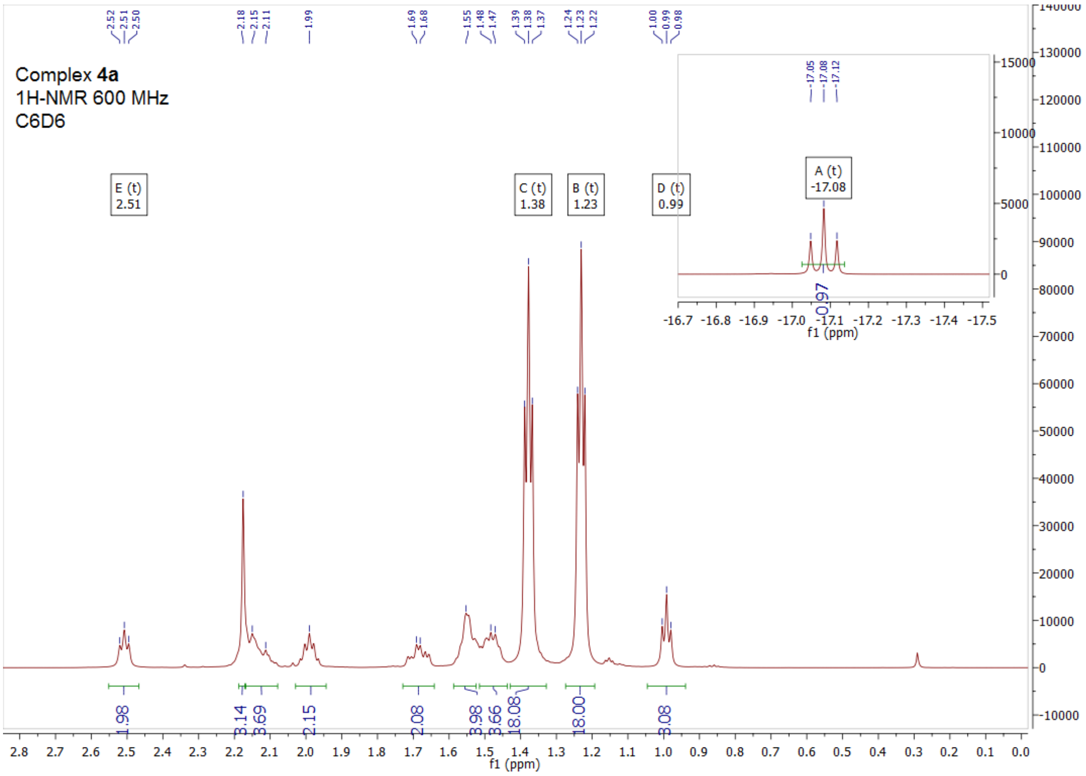

Fig. S17 ^{1}H-NMR of [RuH(CO)(hexanolate)(Me-PNP)] **4a** in C_6D_6 at 600 MHz.

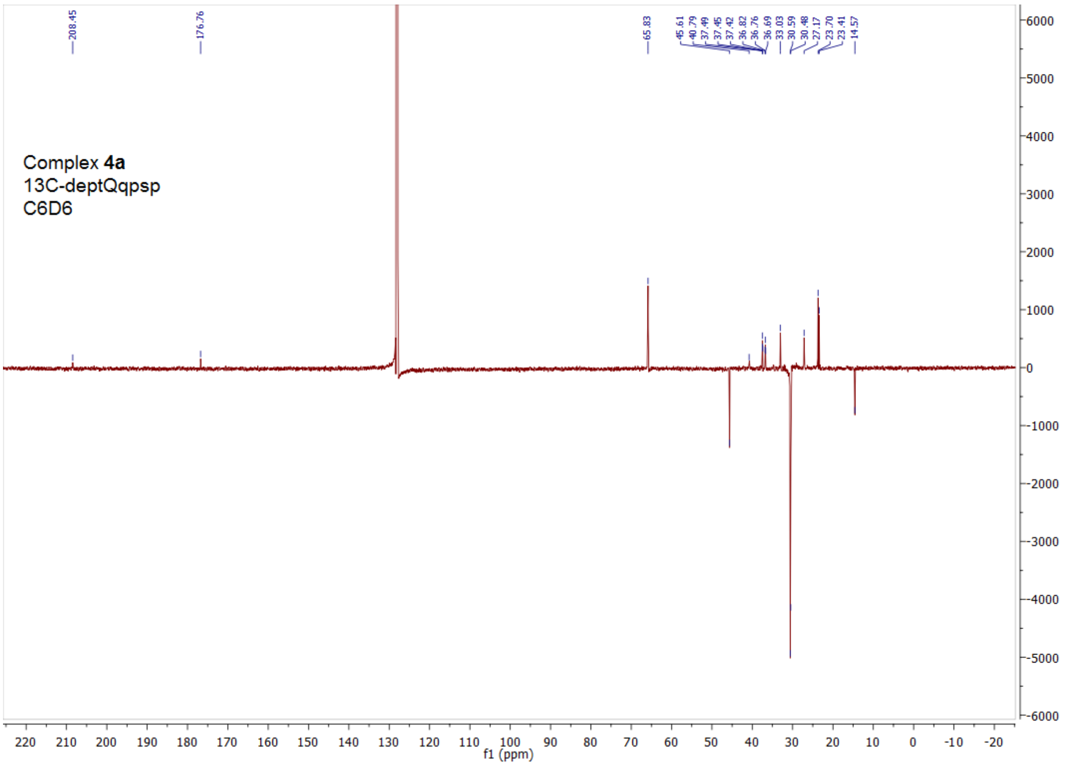

Fig. S18 ^{13}C-deptQ-NMR of [RuH(CO)(hexanolate)(Me-PNP)] **4a** in C_6D_6 at 150 MHz.

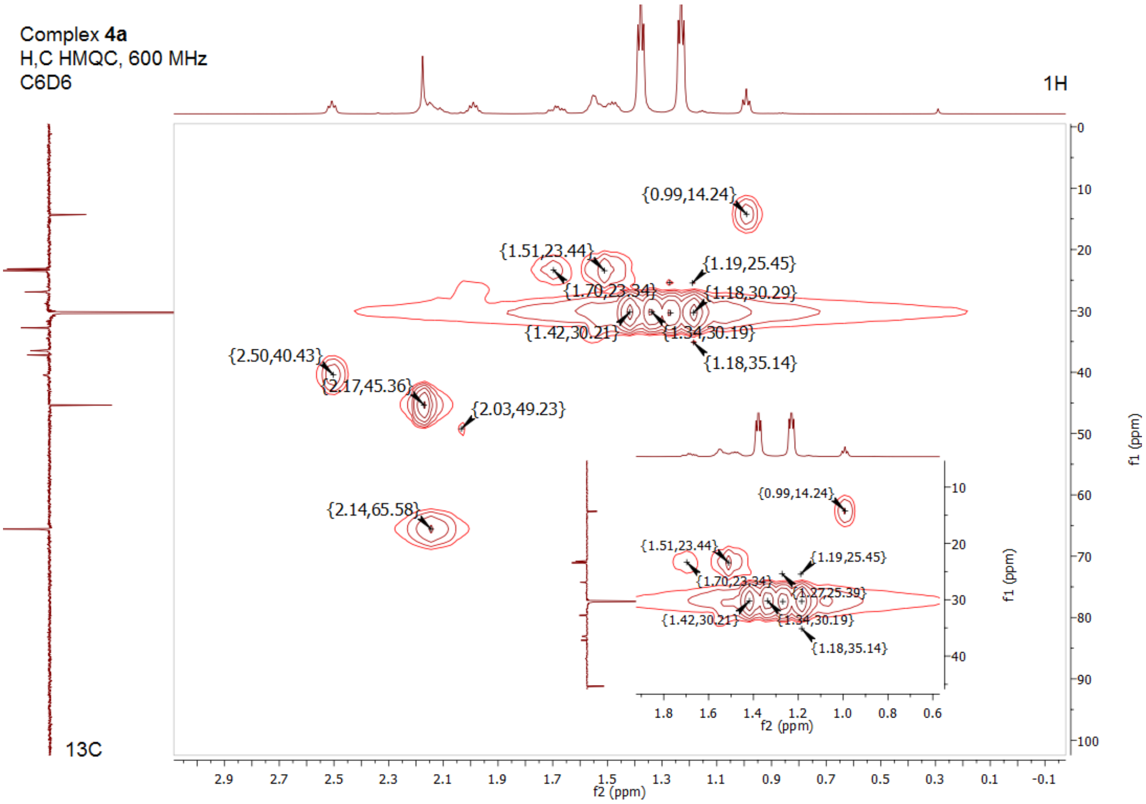

Fig. S19 H,C HMQC of [RuH(CO)(hexanolate)(Me-PNP)] **4a** in C_6D_6 at 600 MHz (^{1}H) 150 MHz (^{13}C).

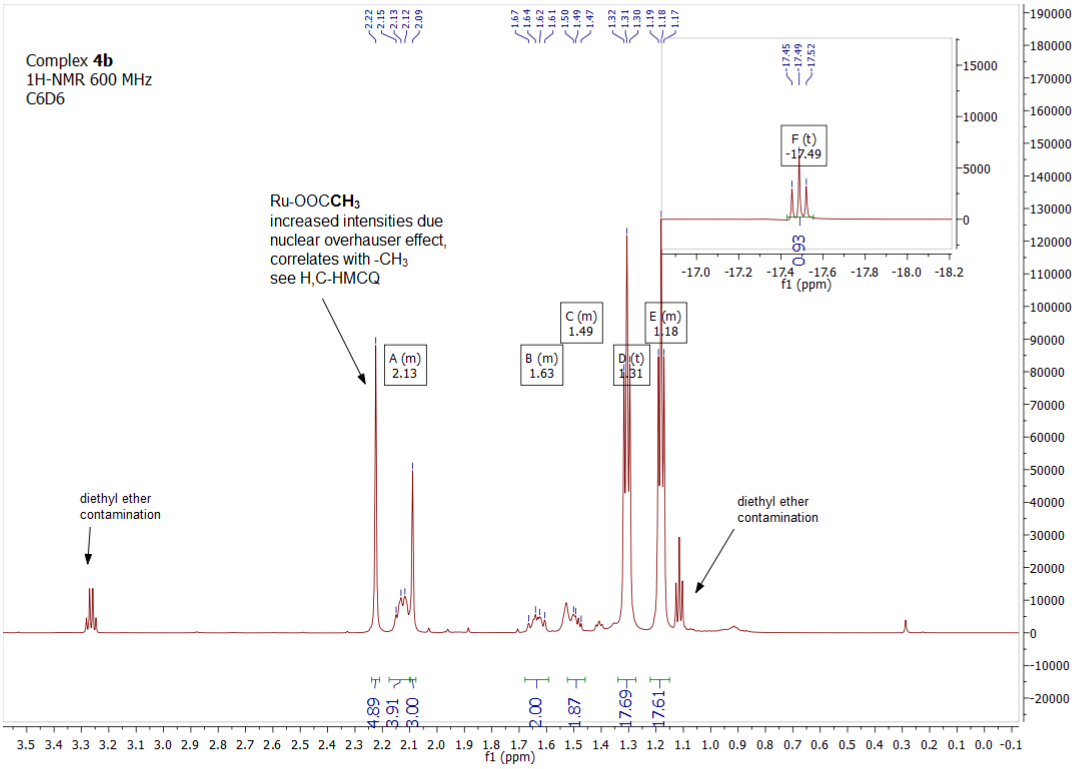

Fig. S20 ^{1}H-NMR of [RuH(CO)(OOCCH$_3$)(Me-PNP)] **4b** in C$_6$D$_6$ at 600 MHz.

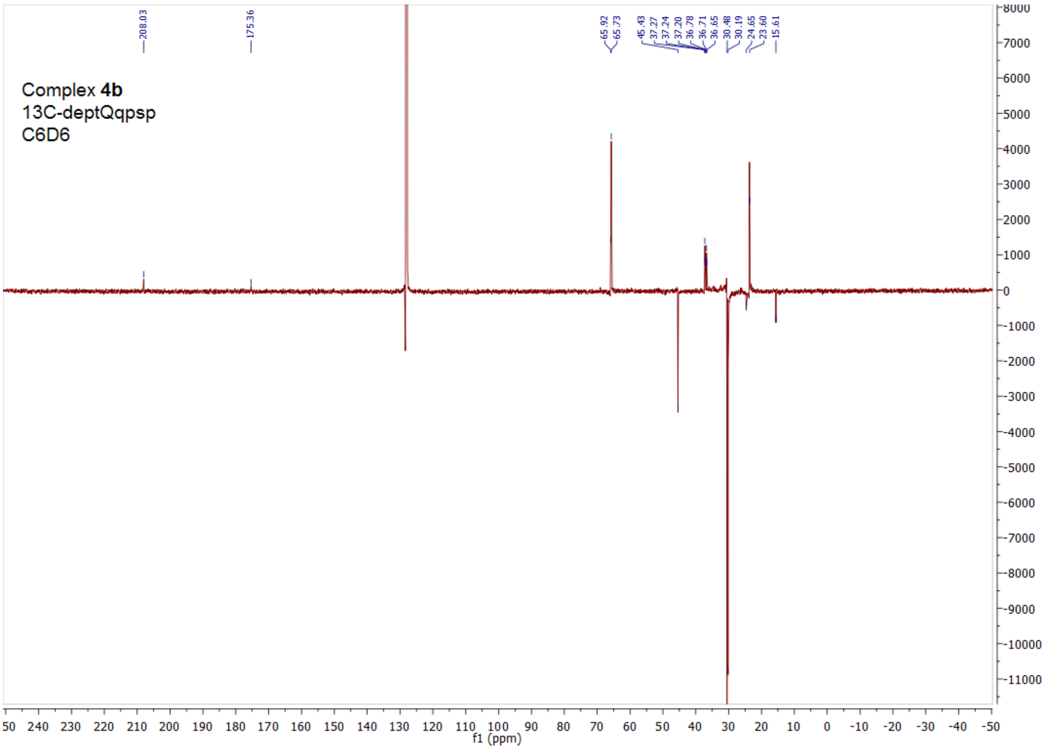

Fig. S21 ^{13}C-deptQ-NMR of [RuH(CO)(OOCCH$_3$)(Me-PNP)] **4b** in C$_6$D$_6$ at 150 MHz.

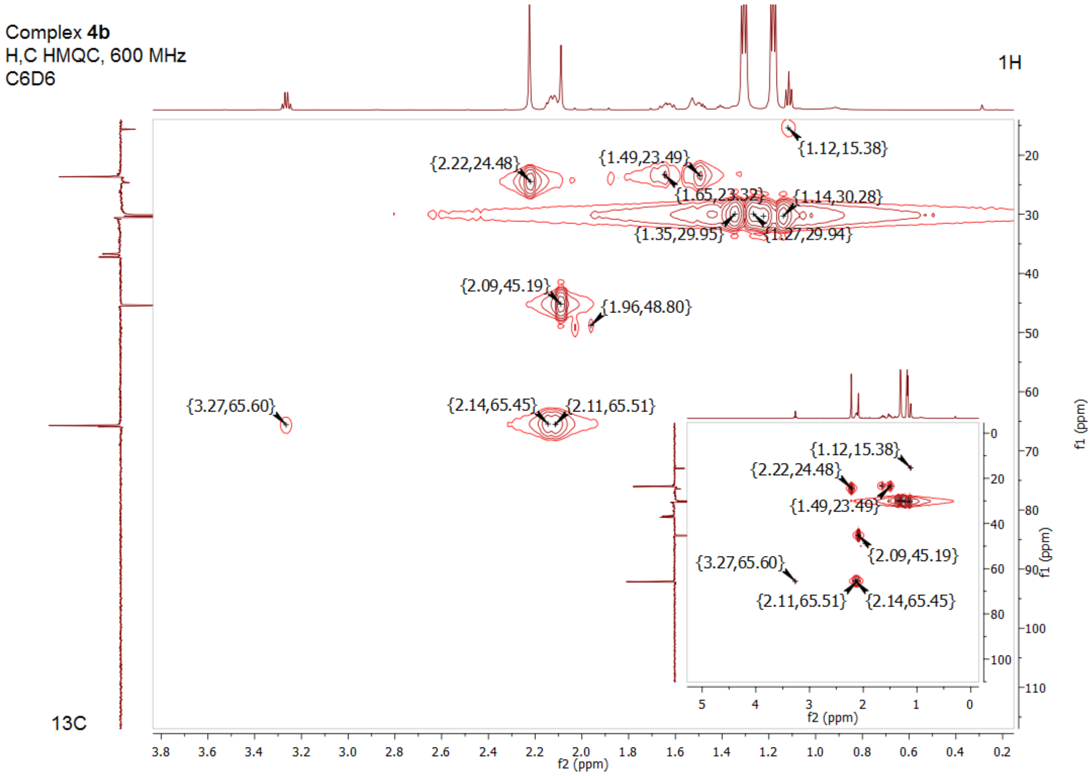

Fig. S22 H,C HMQC of [RuH(CO)(OOCCH$_3$)(Me-PNP)] **4b** in C_6D_6 at 600 MHz (^{1}H)/150 MHz (^{13}C).

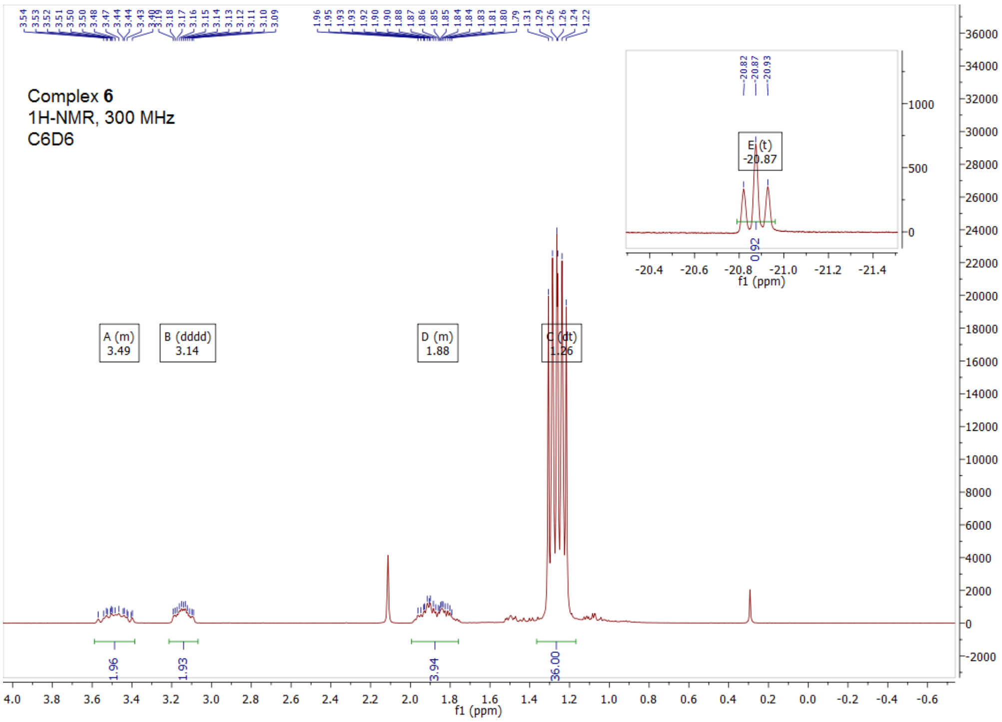

Fig. S23 ^{1}H-NMR of [RuH(CO) (PNP)] **6** in C_6D_6 at 300 MHz.

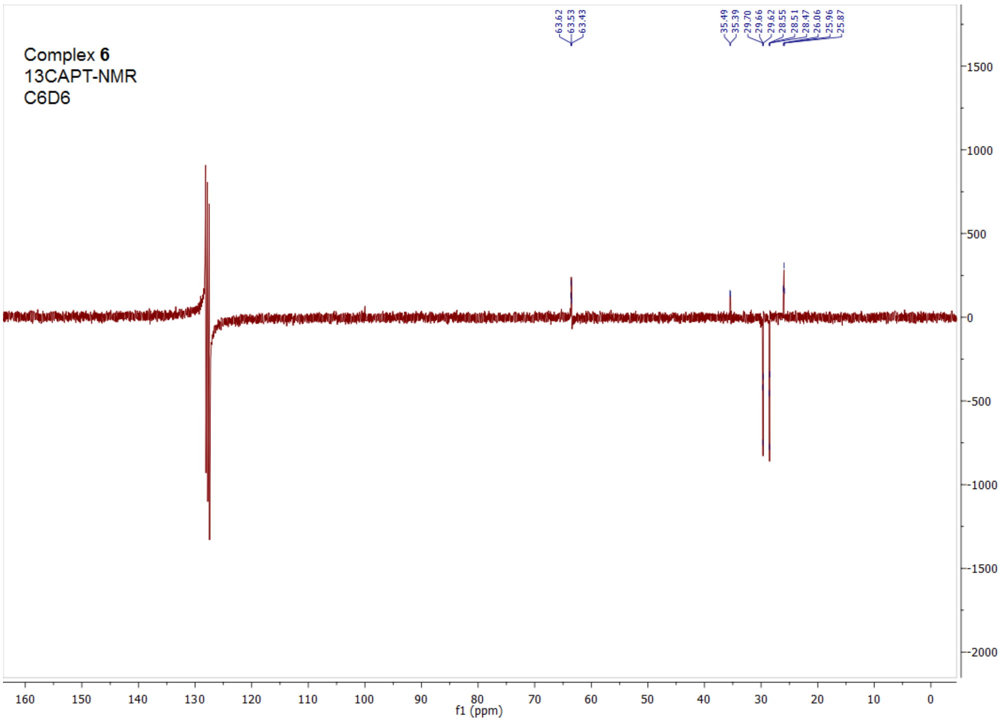

Fig. S24 $^{13}C_{APT}$-NMR of [RuH(CO) (PNP)] **6** in C_6D_6 at 75 MHz.

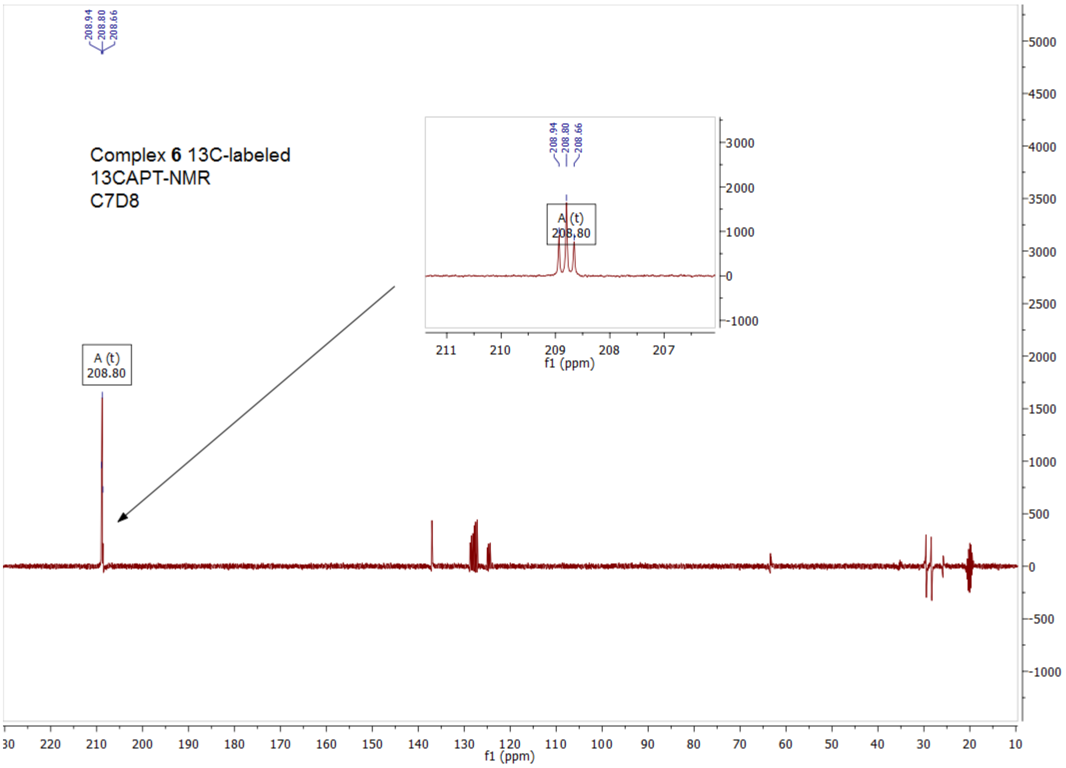

Fig. S 25 $^{13}C_{APT}$-NMR of [RuH(^{13}CO) (PNP)] **6** in C_7D_8 at 75 MHz.

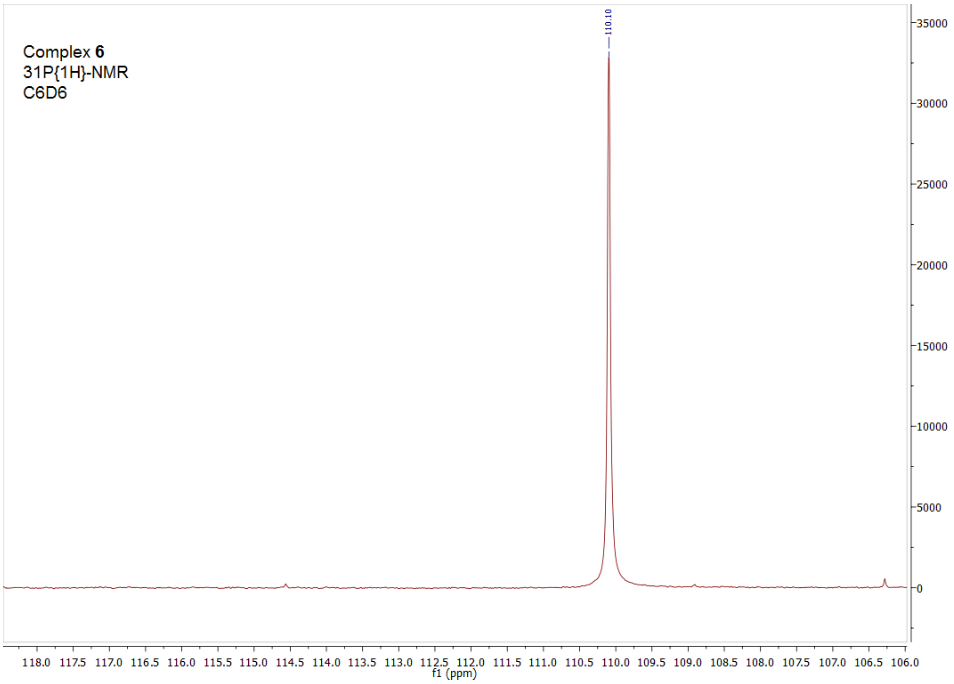

Fig. S26 $^{31}P\{^1H\}$-NMR of [RuH(CO) (PNP)] **6** in C_6D_6 at 121 MHz.

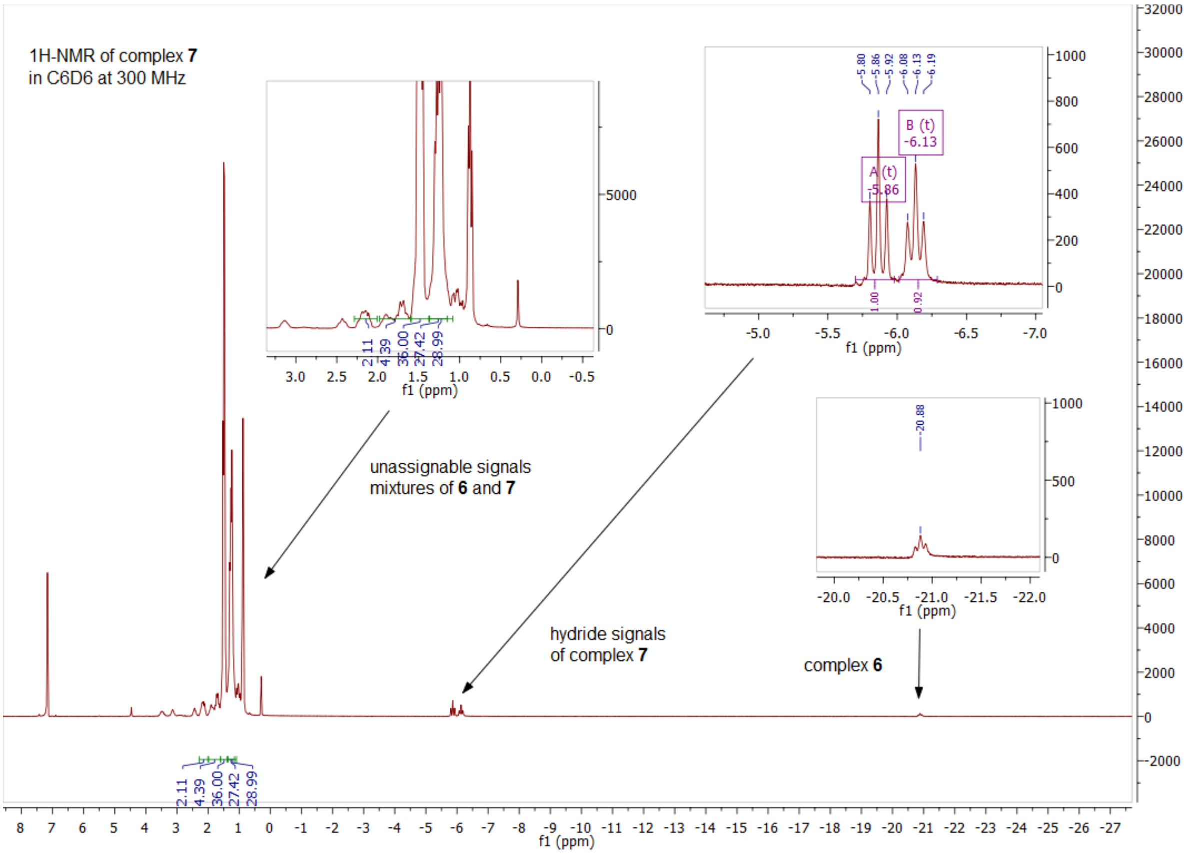

Fig. S27 ^1H-NMR of complex **7** in C_6D_6 at 300 MHz. Hydrogenation of complex **6** to complex **7** with 1.5 bar H_2.

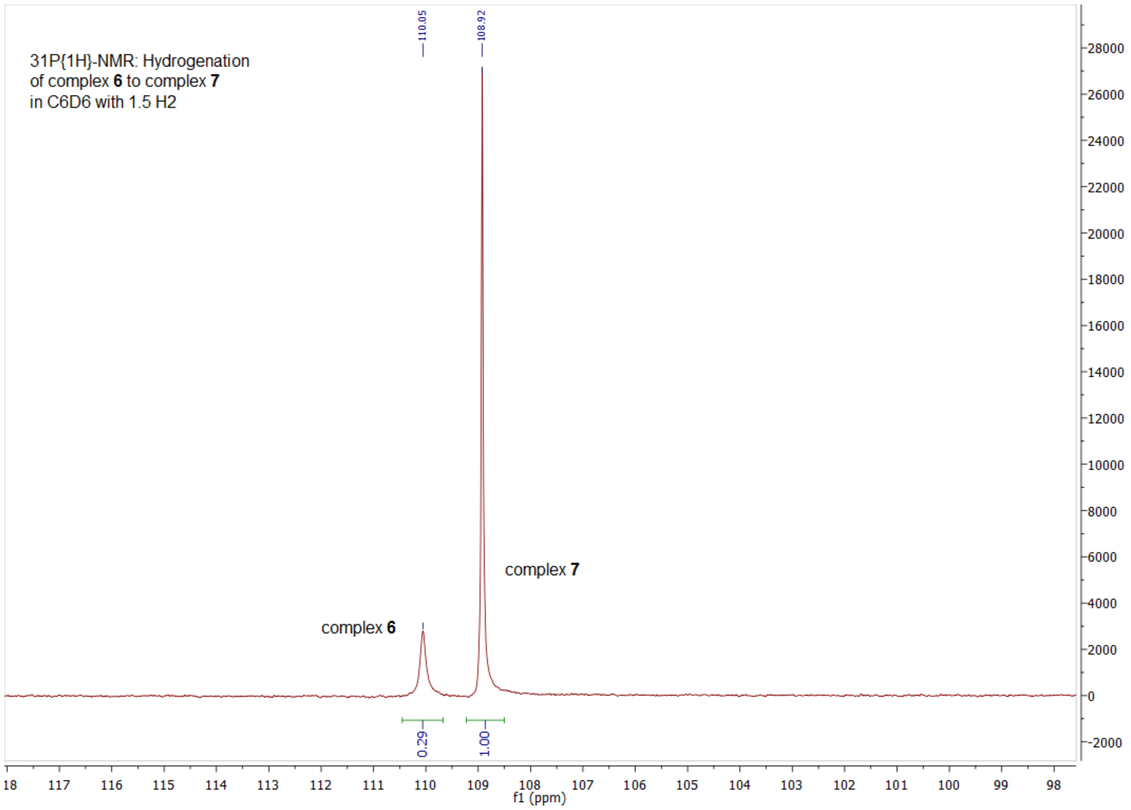

Fig. S28 $^{31}P\{^1H\}$-NMR of complex **7** in C_6D_6 at 121 MHz. Hydrogenation of complex **6** to complex **7** with 1.5 bar H_2, 79% conversion.

5. Single Chrystal structure of complex 4b

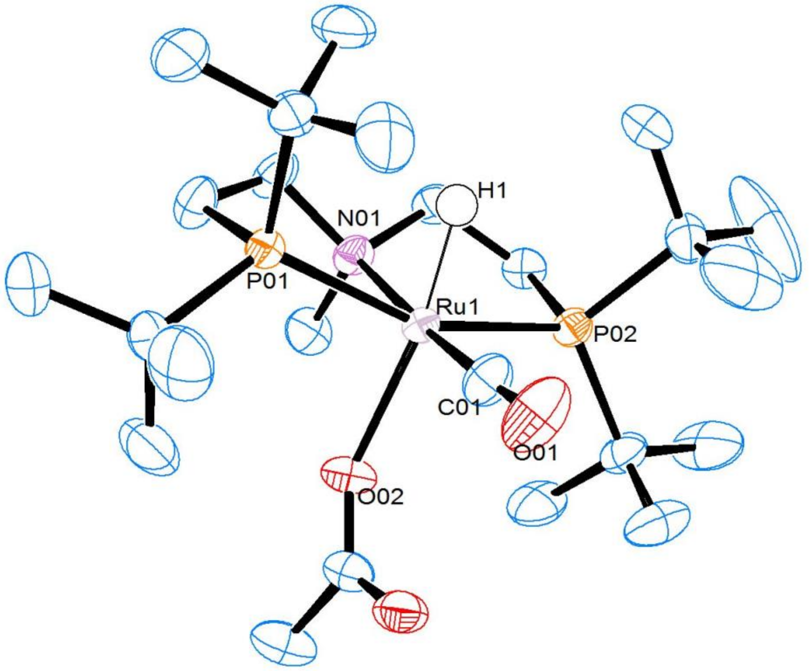

Fig. S29 ORTEP diagram of the single crystal structure of complex **4b**. Ellipsoids are illustrated at 50% possibility. All hydrogen atoms not depicted here except for H1 for clarity**.**

Table 1. Crystal data and structure refinement for shelx.

Identification code	shelx	
Empirical formula	C26 H55 N O5 P2 Ru	
Formula weight	624.72	
Temperature	293(2) K	
Wavelength	0.71073 Å	
Crystal system	Monoclinic	
Space group	P 21/n	
Unit cell dimensions	a = 11.6024(4) Å	α= 90°.
	b = 20.5977(6) Å	β= 113.029(2)°.
	c = 14.1642(4) Å	γ = 90°.
Volume	3115.24(17) Å^3	
Z	4	
Density (calculated)	1.332 Mg/m^3	
Absorption coefficient	0.639 mm^{-1}	
F(000)	1328	
Crystal size	? x ? x ? mm^3	
Theta range for data collection	1.849 to 26.789°.	
Index ranges	-14<=h<=14, -25<=k<=26, -17<=l<=17	
Reflections collected	31157	

Independent reflections	6585 [R(int) = 0.0394]
Completeness to theta = 25.242°	100.0 %
Refinement method	Full-matrix least-squares on F^2
Data / restraints / parameters	6585 / 0 / 316
Goodness-of-fit on F^2	1.027
Final R indices [I>2sigma(I)]	R1 = 0.0308, wR2 = 0.0780
R indices (all data)	R1 = 0.0376, wR2 = 0.0823
Extinction coefficient	n/a
Largest diff. peak and hole	0.701 and -0.620 e.Å^{-3}

Table 2. Atomic coordinates (x 10^4) and equivalent isotropic displacement parameters (Å^{2}x 10^3) for shelx. U(eq) is defined as one third of the trace of the orthogonalized U^{ij} tensor.

	x	y	z	U(eq)
Ru(1)	2715(1)	1478(1)	7506(1)	23(1)
P(02)	1067(1)	1667(1)	8038(1)	26(1)
P(01)	4037(1)	874(1)	6936(1)	26(1)
O(03)	3880(2)	3090(1)	7651(1)	41(1)
O(02)	2581(2)	2371(1)	6594(1)	36(1)
O(01)	4724(2)	1916(1)	9466(2)	58(1)
N(01)	1177(2)	1077(1)	6100(1)	28(1)
C(02)	3108(2)	2915(1)	6786(2)	34(1)
C(17)	595(2)	2531(1)	8155(2)	37(1)
C(07)	5311(2)	1257(1)	6601(2)	37(1)
C(21)	1115(2)	1175(1)	9194(2)	37(1)
C(04)	665(2)	1567(1)	5269(2)	39(1)
C(05)	1617(2)	502(1)	5687(2)	39(1)
C(01)	3947(2)	1755(1)	8691(2)	37(1)
C(11)	4689(3)	112(1)	7703(2)	40(1)
C(15)	133(2)	837(1)	6378(2)	32(1)
C(16)	-296(2)	1332(1)	6960(2)	32(1)
C(13)	5374(3)	290(2)	8833(2)	57(1)
C(19)	273(3)	2851(2)	7110(2)	54(1)
C(06)	2916(2)	593(1)	5682(2)	40(1)
C(22)	1313(4)	466(2)	9042(3)	66(1)
C(12)	5554(3)	-282(2)	7327(3)	51(1)
C(08)	4850(4)	1922(2)	6171(3)	66(1)
C(03)	2777(3)	3382(2)	5893(2)	50(1)

C(09)	5676(3)	883(2)	5830(3)	56(1)
C(14)	3605(3)	-345(1)	7622(3)	59(1)
C(10)	6494(3)	1354(2)	7585(3)	63(1)
C(20)	1724(3)	2883(2)	8931(3)	57(1)
C(18)	-538(4)	2622(2)	8429(4)	79(1)
C(24)	-66(5)	1211(3)	9394(4)	133(3)
C(23)	2220(5)	1391(2)	10138(3)	98(2)
O(201)	-192(2)	796(1)	2858(2)	39(1)
O(200)	1496(2)	253(1)	3002(2)	56(1)
C(101)	948(2)	764(1)	2880(2)	37(1)
C(100)	1527(3)	1392(2)	2756(3)	53(1)